The International Journal of Advanced Manufacturing Technology
https://doi.org/10.1007/s00170-022-09603-4

ORIGINAL ARTICLE

Influence of drawbead geometry and blank holder force on the dual phase steel formability

Alex Raimundo de Oliveira[1] · Sérgio Fernando Lajarin[1] · Claudimir José Rebeyca[1] · Ravilson Antonio Chemin Filho[1] · Chetan P. Nikhare[2] · Paulo Victor Prestes Marcondes[1]

Received: 9 February 2022 / Accepted: 23 June 2022

Abstract
Mostly, stamping industries, especially the automobile, uses a single machine to manufacture several parts. As a result, a time to try out stamping tools to start a new production cycle is often necessary. To reach the expected degree of satisfaction for the product, the tryout involves: choosing a material with better formability, adjustments in the design of punches, dies, and components that assemble the tooling. For this, the development of laboratory tests, which allows a better understanding of material stamp-ability and the influence of tooling parameters, become essential for smooth preparation for production and the development of more accurate computational models. Given these challenges, the present work studies the influence of the drawbead geometry and the blank holder force (BHF) on the stampability of DP780 steel. For this, an interchangeable drawbead system was developed for a Nakazima test tool. The four drawbead geometries were used: flat (without salience projection), circular, triangular, and square. In addition, three-level of BHF were used. For each set of drawbead geometry and BHF, the forming limit curve (FLC) of DP780 steel was obtained and analyzed. From the results, it was possible to observe the best configuration of drawbead and BHF. Furthermore, the results showed clear gains in formability and the influence of drawbead geometry and BHF on the DP780 stamping.

Keywords Drawbead · Blank holder force · Forming limit curve · DP780

1 Introduction

Analyzing the needs of the automotive industry, it can be said that the current scenario points to a constant search for improvements in several aspects, among which are vehicle performance, safety, reduction in pollution rates and design, associated with better productivity, and cost reduction. To meet this industry need, improving the vehicle body becomes very relevant since all the parts that make up the car are contained, in addition to the occupants themselves. Focusing on the bodywork, some studies are directed to the use of materials and alternative processes currently used and their feasibility; Spreafico [1], Sun et al. [2, 3], Pattarakunnan et al. [4], Roy et al. [5], and Vita et al. [6]. This discussion points out possible alternative materials for the manufacture of more ecological bodies for current vehicles, combustion, electric, or hybrid. Bearing in mind, however, the manufacturing unfeasibility of alternative processes, stamping continues to be of fundamental importance for the production of the bodywork, which strengthens studies in this aspect. It is worth mentioning that the stamping process, used for the production of body components from sheet metal, suits the mass production demand of automakers, while other alternative manufacturing processes may not meet this demand.

In this way, the improvement of the bodywork to meet the current needs of the automotive industry implies the advancement of studies aimed at three segments: AHSS steels [7–13], design, and processing. The improvement of these three lines of research, however, depends directly on the development of more sophisticated methods of analysis regarding the behavior of materials during stamping, where the Nakazima stamping test stands out, whose main objective is to determine the forming limit curve of metal sheets.

✉ Chetan P. Nikhare
cpn10@psu.edu

[1] Mechanical Engineering Department, Federal University of Paraná, Curitiba PR, Brazil

[2] Mechanical Engineering Department, Pennsylvania State University, Erie, PA, USA

Published online: 19 July 2022

The forming limit curve (FLC) refers to a classic and accurate instrument for predicting the sheet metal maximum formability limit. Developed by authors such as Keeler [14], Goodwin [15], and Woodthorpe and Pearce [16], it also serves as a working tool for several authors, with different purposes. The method proposed by Min et al. [17], evaluated the appearance of localized cracks through a change in the curvature of the sheet metal surface. Affronti and Merklein [18] also focused their study on a method of failure analysis of metal sheets in different states of stress measured at the surface of the material, through Nakazima tests and the forming limit curve, while Barlo et al. [9] worked on the development of an experimental method to obtain the FLC of sheet metal using digital image correlation and an optical technique, allowing for more accurate measurement of the displacement and deformation of points across the surface of the sample. Other works that used the FLC and the Nakazima stamping test for its realization, which can still be mentioned, are the one by Schmid et al. [13], focusing on the behavior of failures in the mechanical forming process, and Iquilio et al. [19] who involved in their analysis the traditional FLC and a nonlinear FLC model. Shinmiya et al. [20] used the forming limit curve to detect possible failures and/or occurrence of bending cracks by stretching on sheet metal surfaces with different flexibilities. Norz and Volk [21] used the traditional Nakazima test to evaluate the model developed by Jocham et al. [22] by comparing the curves obtained.

Following another study direction, focusing on the effect that the stamping tool variables provide on the sheet stampability limit, it is worth highlighting the work of Chemin Filho [23], who showed a significant increase in the formability limit of DP600 steel due to a more assertive choice of blank holder force (BHF), and Shinmiya et al. [20], a study in which the increase in the holding force on the blank promoted an increase in the maximum stress of the tested materials. Affronti and Merklein [18] and Sarraf et al. [24] reinforce the effect of tool variables on the stampability of AHSS steels. In addition to the BHF, the drawbead (DB) is also of fundamental importance in the determination of the sheet metal limit of formability, as it acts directly on the restriction to the flow of the sheet during forming, defining, together with the BHF, the deformation mode suffered by the material [25, 12]. In this way, it is concluded that the characteristics of the tooling have a strong effect on the stamping process, promoting a microstructural transformation [26], Fig. 1, that directly affects the degree of formability of the sheet. An example of this is the Bauschinger effect, like studied by [27], Fig. 2.

Paul [28], assuming the FLC as a precise instrument for evaluating the stampability of sheet metal, due to the sensitivity presented to the properties of the materials and regarding the stamping tools variables, proposed in his work the practical use of forming limit curves as an instrument to quantify the formability of the DP780 steel sheet in different configurations of the Nakazima test tool. In this case, by varying the force of the blank holder and the geometry of the drawbead, was became possible to show that these tool variables have a direct effect on the performance of the material during stamping, demystifying the common shop floor concepts and techniques, which are not take this aspect into account in their analysis, Fig. 3.

In this way, the main contribution/innovation of the proposed work is to make the analysis more sophisticated regarding the effect of the tool variables on the sheet forming limit, making it possible to quantify the performance of the material according to the configuration of the stamping tool, serving as a basis for a safer and more accurate assessment during tool design and correction of processing failures in the industry.

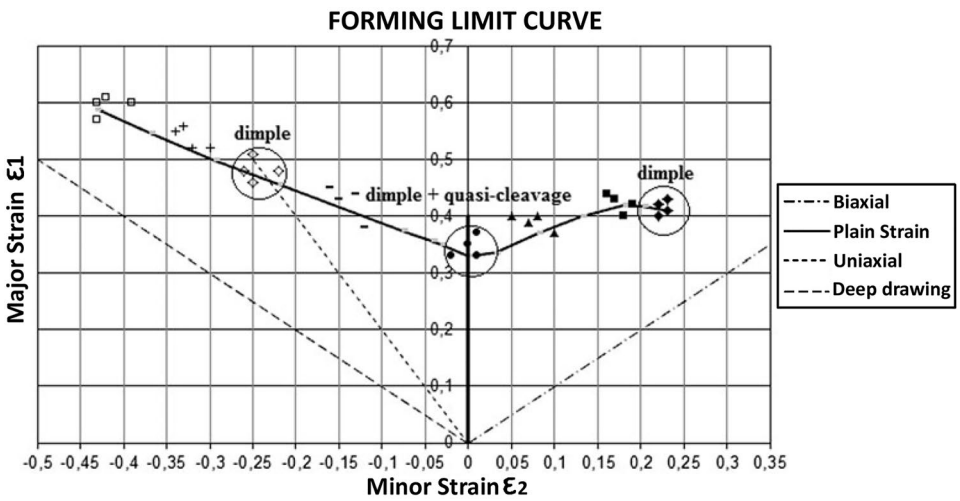

Fig. 1 Proposed DP600 FLC related to the micromechanisms of fracture generated by uniaxial, biaxial tensile stress and plane strain states [26]

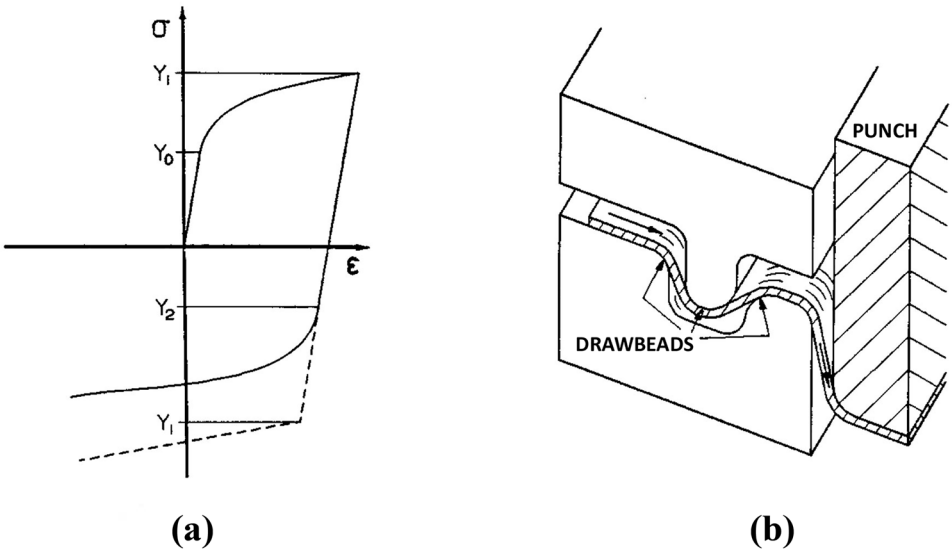

Fig. 2 Bauschinger curve (**a**); sheet metal flow by drawbead (**b**) [27]

2 Methodology

The material used in this work was the Dual Phase 780 (DP780) with a thickness of 1.5 mm. Table 1 shows the material properties of DP780 steel.

To obtain the FLC, the Nakazima test was performed. According to ISO 12004–2 [29], at least five geometries for the description of a complete FLC are necessary. For the present work, sets containing eight specimens were used, all with 200 mm in length and widths of 70, 80, 90, 100, 125, 150, 175, and 200 mm, according to Fig. 4.

This number of specimens was considered sufficient for the expected purpose. The tests were repeated three times for each condition and were referring to the four drawbead geometries (plane, circular, triangular, and square) and the three BHFs 569, 785, and 1157 kN, making 36 sets and a total of 288 samples. Once the sheet metal is cut in shape and cleaned, a circle grid of 5 mm was printed using a silk screen method. The printing mixture was composed of 90% of epoxy paint and 10% of nitric acid. The printed circle grid on the sheet metal was used to measure the strains occurred during the stamping process. The preparation of the samples

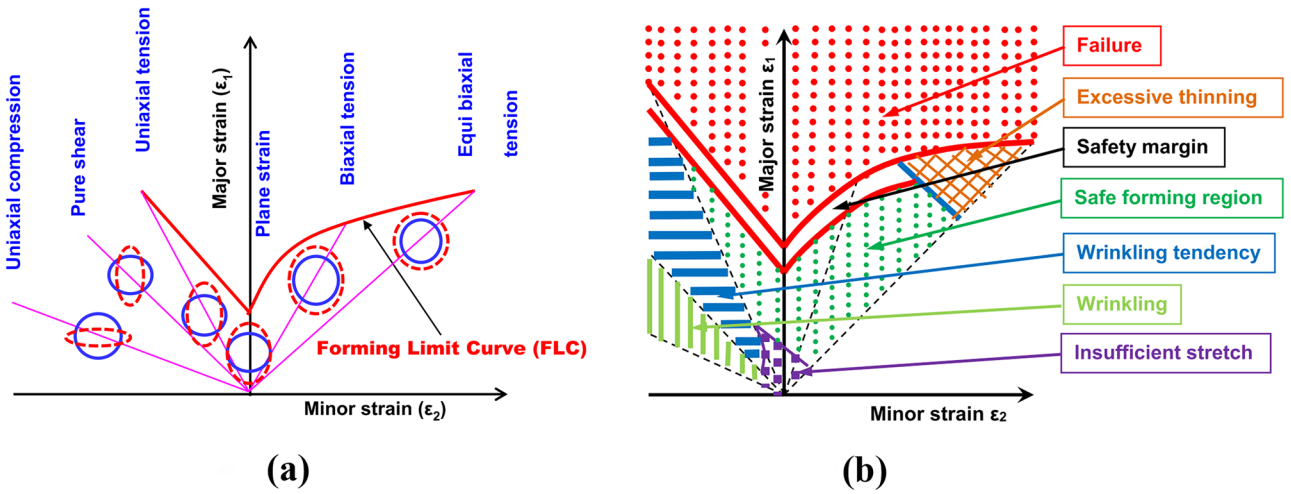

Fig. 3 Schematic forming limit curve (FLC) with diferente strain states (**a**); schematic forming limit diagram (FLD) representing safe forming zone (**b**) [28]

Table 1 Material mechanical properties (Arcelor Mittal 2021)

DP 780 Steel				
Properties	**0°**	**45°**	**90°**	**Average value**
0.2% YS (MPa)	530	526	549	535
UTS (MPa)	793	783	802	793
UE (%)	13.7	14.5	12.5	13.6
TE (%)	20.8	21.7	18.1	20.2
r value	0.68	1.06	0.95	0.897
n value	0.144	0.153	0.138	0.145

YS yield strength, *UTS* ultimate tensile strength, *UE*, uniform elongation, *TE* total elongation, *r* coefficient of plastic anisotropy, *n* strain hardening coefficient

and the measurement after de tests were performed according to Chemin Filho et al. [30]. The circle grids were also used to identify the rupture location for each specimen. The profile and dimensions of four drawbead geometries, P (plane "smooth surface") or flat drawbead, C (circular), T (triangular), and Q (square) are shown in Fig. 5. Figure 6 shows the assembly of the Nakazima test tool, which is composed of the die, punch, and BHF. The configuration of this tool also allows for changing the drawbead geometries. The tools are coupled to a hydraulic press, controlled by software which regulates the force of the BHF and the speed of the punch.

3 Results and discussion

3.1 Fracture analysis

After each stamping test, five different situations were observed depending on the location of the crack in the tested sample, Fig. 7.

The legend in Fig. 7 classifies each of the crack locations that occurred in the tests by color. It should be noted that the only condition that allows the measurement of major and minor strains for the FLC determination is the crack located in the punch radius region (defined by the green color). All other conditions imply the disposal of the specimen, i.e., total slip without a crack (yellow), crack in the die shoulder (red), crack in the drawbead (purple), and cracks between the drawbead and the die shoulder (blue). Based on the above categorization, the samples were detailed in Table 2. Table 2 also shows the sequence of the eight stamped specimens for each drawbead geometry and each BHF condition. Through this mapping, it is possible to observe the location of the crack generated in each specimen depending on the drawbead and BHF used.

According to Table 2, it can be noted that the specimens with widths of 200, 175, and 150 mm have the crack located in the region of the punch radius (green color) for all drawbead geometries and for all BHF conditions. Thus, it can be

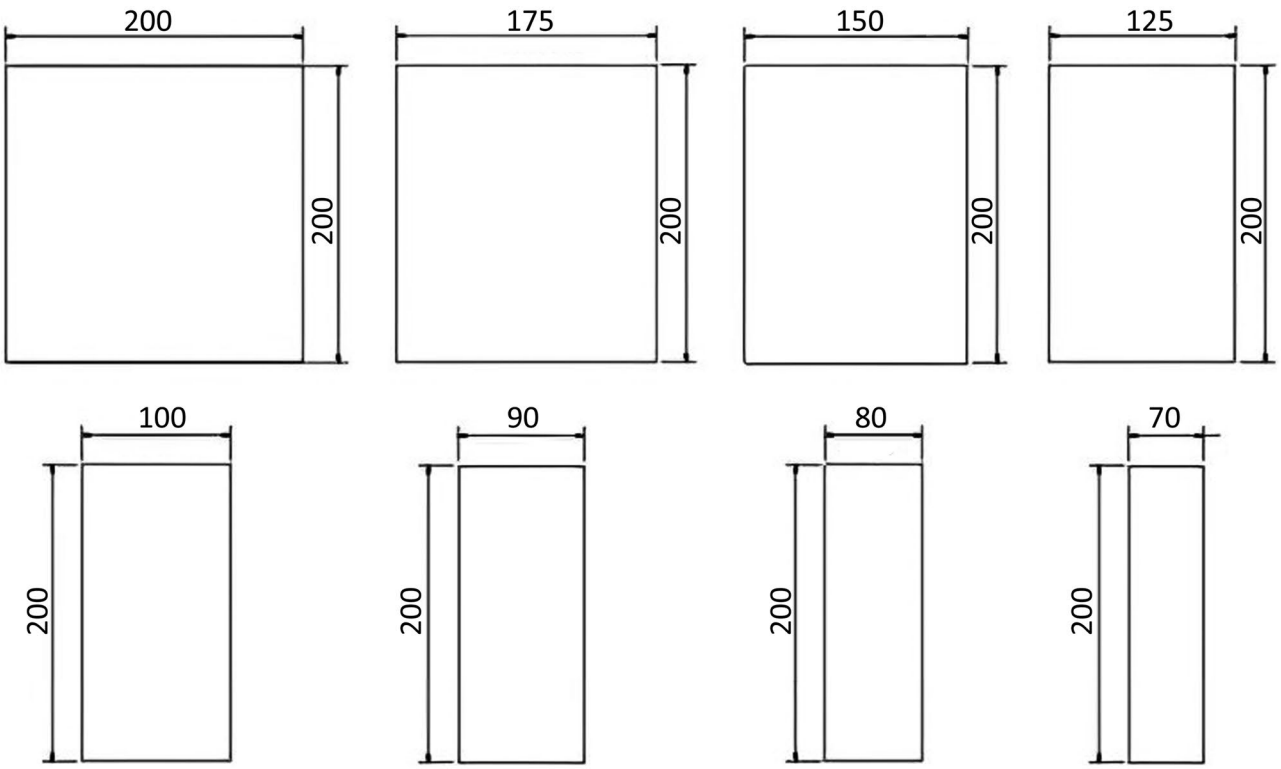

Fig. 4 Specimen's geometries carried out on Nakazima's tests

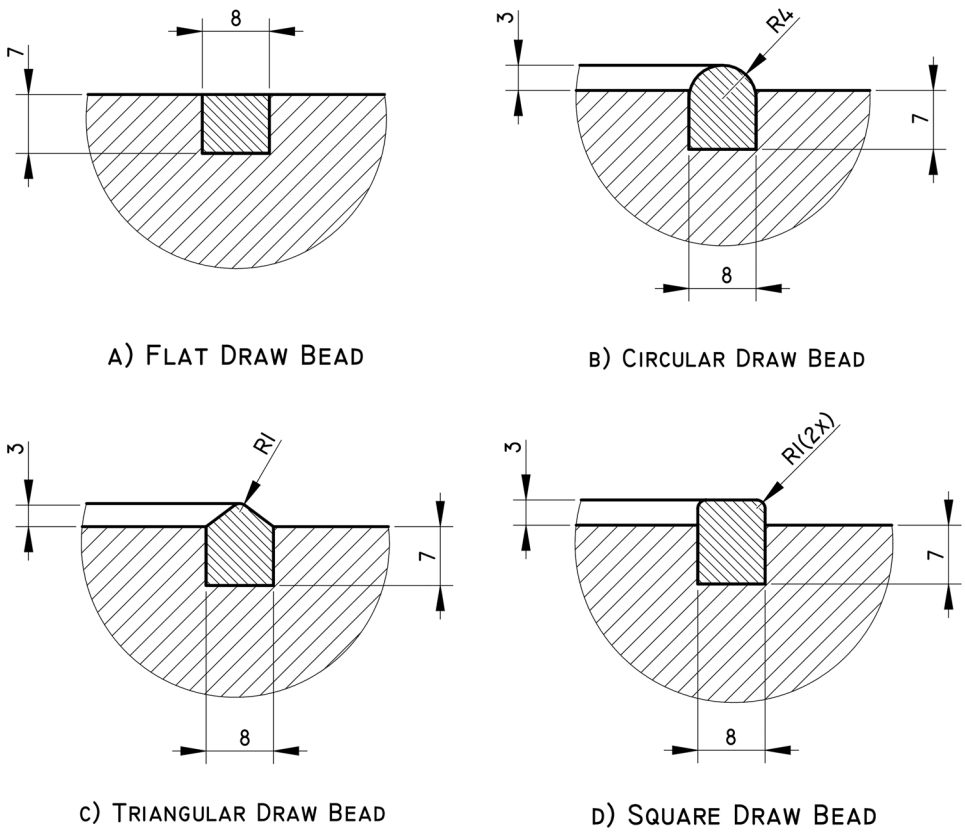

Fig. 5 Details and dimensions of the drawbead geometries: **a** flat drawbead, **b** circular drawbead, **c** triangular drawbead, and **d** square drawbead

assumed that the stretch deformation mode predominates in these specimens where there is a greater restriction imposed by the BHF. The crack location in these specimens can be called as "ideal" since the crack located in the region of the punch radius, which leads to a better performance of the material in terms of stamp-ability. In other words, it is in

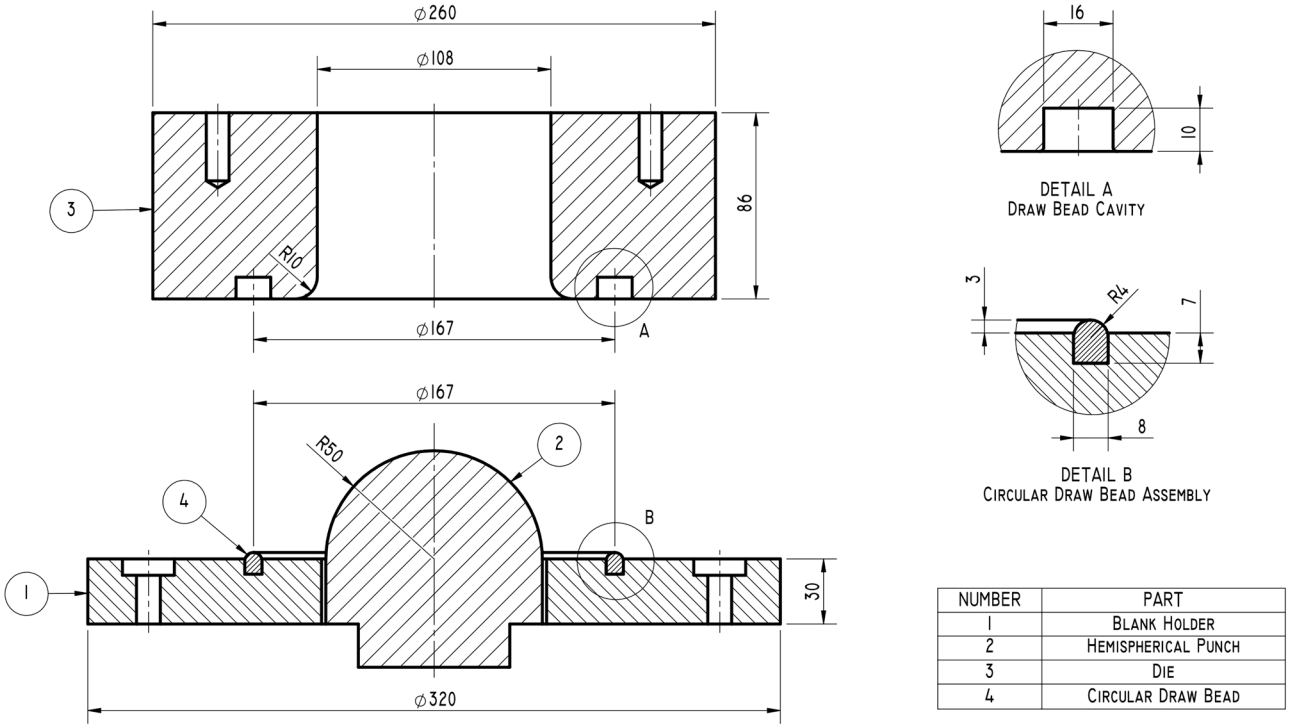

NUMBER	PART
1	BLANK HOLDER
2	HEMISPHERICAL PUNCH
3	DIE
4	CIRCULAR DRAW BEAD

Fig. 6 Modified Nakazima test tool, with interchangeable drawbead rings

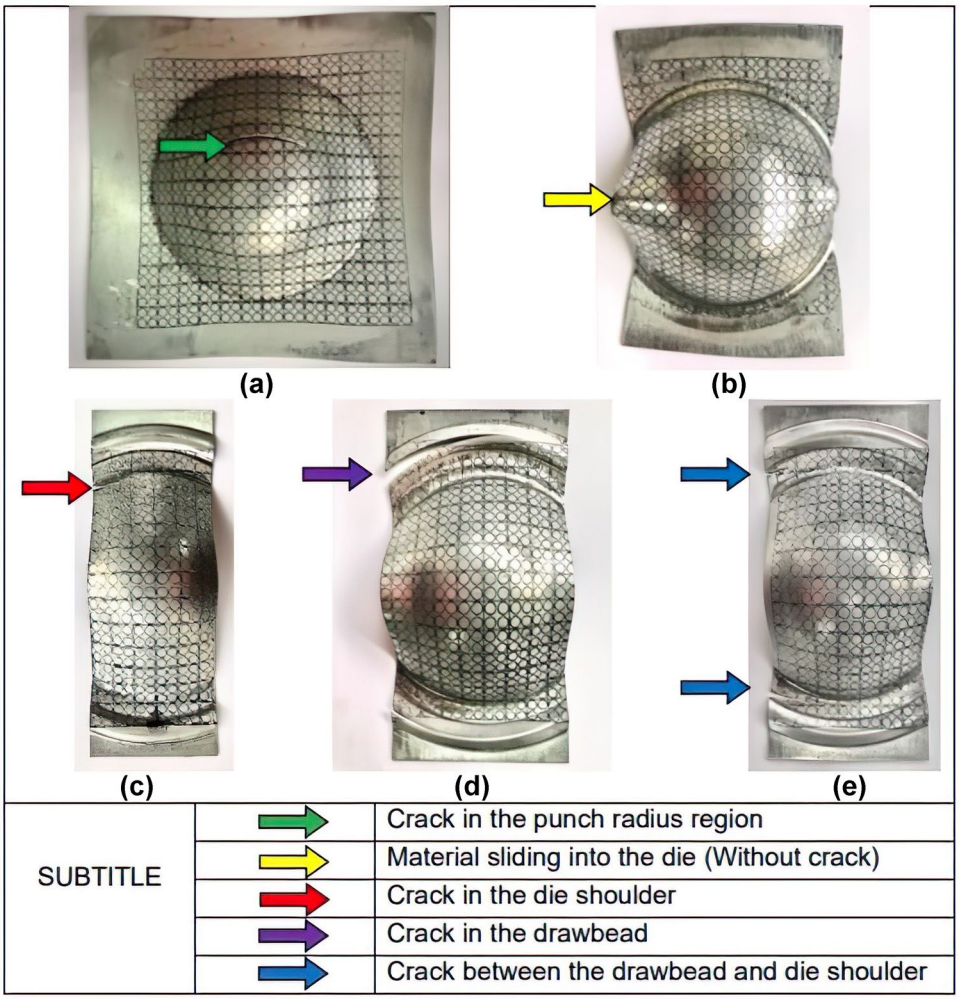

Fig. 7 Classification according to the crack location after the Nakazima stamping tests: **a** crack in the punch radius region, **b** material sliding into the die (without crack), **c** crack in the die shoulder, **d** crack in the drawbead, and **e** crack between the drawbead and the die shoulder

the condition where the sheet reaches the highest levels of deformation until the occurrence of the crack (more satisfactory for stamping operations).

For the specimens with widths of 125 and 100 mm, the circle deformation is close to the plane strain state. In these widths' samples, not all fracture occurred in the punch radius region (green color), which puts them in the transition zone. For the flat drawbead, with a BHF of 569 kN, there was a total slip of the material. The triangular drawbead cracked the samples on the die shoulder at 569 kN for the 100 mm wide specimen and in the drawbead region for the BHF of 785 and 1157 kN (for the same specimen width).

In the case of the flat drawbead, where there is no salience restriction, the load of 569 kN proved to be insufficient to restrict the sheet flow, to the point of causing it to break. This characterizes a poor use of the material's stampability. In addition, the complete advancement of the material into the die can result in the crushing of the sheet during the process resulting in a scrap. Also, this situation induces the scratch marks on the die. Thus, it can be suggested to use the BHF above 569 kN for this drawbead. In the case of the triangular drawbead with 100 mm width specimens, all failed at the die shoulder or at the drawbead. The triangular drawbead geometry promotes hardening and a concentration of more accentuated stresses on the material, so that, for 569 kN BHF, the material flows to the point where the crack evolves over the die shoulder. For the conditions of 785 and 1157 kN, cracking already occurs in a catastrophic manner in the drawbead itself, without further evolution of the sheet stamping.

For sample widths less than 100 mm (90-, 80-, and 70-mm width), where the predominant deformation mode is by deep drawing, the vast majority of specimens did not evolve into a rupture in the punch radius. Thus, practically all drawbead geometries and BHF were used, and the samples were disapproved for the FLC, therefore called the "critical region" in Table 2. With the flat drawbead, the material has greater freedom of flow due to the nonexistence of the salience in the BHF, and thus all the failed test specimens presented a crack over the die shoulder. For the circular drawbead, the failed specimens presented an alteration in the position of the crack, varying between the

Table 2 Crack mapping in stamped specimens

		IDEAL REGION									TRANSITION REGION						CRITICAL REGION								
FLAT DRAWBEAD (SMOOTH SURFACE)	Sample dimensions	200X200 mm			200x175 mm			200x150 mm			200x125 mm			200x100 mm			200x90 mm			200x80 mm			200x70 mm		
	BH Force/Samples	1	2	3	1	2	3	1	2	3	1	2	3	1	2	3	1	2	3	1	2	3	1	2	3
	569 KN	P1	P2	P3	P4	P5	P6	P7	P8	P9	P10	P11	P12	P13	P14	P15	P16	P17	P18	P19	P20	P21	P22	P23	P24
	785 KN	P25	P26	P27	P28	P29	P30	P31	P32	P33	P34	P35	P36	P37	P38	P39	P40	P41	P42	P43	P44	P45	P46	P47	P48
	1157 KN	P49	P50	P51	P52	P53	P54	P55	P56	P57	P58	P59	P60	P61	P62	P63	P64	P65	P66	P67	P68	P69	P70	P71	P72
CIRCULAR DRAWBEAD	Sample dimensions	200X200 mm			200x175 mm			200x150 mm			200x125 mm			200x100 mm			200x90 mm			200x80 mm			200x70 mm		
	BH Force/Samples	1	2	3	1	2	3	1	2	3	1	2	3	1	2	3	1	2	3	1	2	3	1	2	3
	569 KN	C1	C2	C3	C4	C5	C6	C7	C8	C9	C10	C11	C12	C13	C14	C15	C16	C17	C18	C19	C20	C21	C22	C23	C24
	785 KN	C25	C26	C27	C28	C29	C30	C31	C32	C33	C34	C35	C36	C37	C38	C39	C40	C41	C42	C43	C44	C45	C46	C47	C48
	1157 KN	C49	C50	C51	C52	C53	C54	C55	C56	C57	C58	C59	C60	C61	C62	C63	C64	C65	C66	C67	C68	C69	C70	C71	C72
TRIANGULAR DRAWBEAD	Sample dimensions	200X200 mm			200x175 mm			200x150 mm			200x125 mm			200x100 mm			200x90 mm			200x80 mm			200x70 mm		
	BH Force/Samples	1	2	3	1	2	3	1	2	3	1	2	3	1	2	3	1	2	3	1	2	3	1	2	3
	569 KN	T1	T2	T3	T4	T5	T6	T7	T8	T9	T10	T11	T12	T13	T14	T15	T16	T17	T18	T19	T20	T21	T22	T23	T24
	785 KN	T25	T26	T27	T28	T29	T30	T31	T32	T33	T34	T35	T36	T37	T38	T39	T40	T41	T42	T43	T44	T45	T46	T47	T48
	1157 KN	T49	T50	T51	T52	T53	T54	T55	T56	T57	T58	T59	T60	T61	T62	T63	T64	T65	T66	T67	T68	T69	T70	T71	T72
SQUARE DRAWBEAD	Sample dimensions	200X200 mm			200x175 mm			200x150 mm			200x125 mm			200x100 mm			200x90 mm			200x80 mm			200x70 mm		
	BH Force/Samples	1	2	3	1	2	3	1	2	3	1	2	3	1	2	3	1	2	3	1	2	3	1	2	3
	569 KN	Q1	Q2	Q3	Q4	Q5	Q6	Q7	Q8	Q9	Q10	Q11	Q12	Q13	Q14	Q15	Q16	Q17	Q18	Q19	Q20	Q21	Q22	Q23	Q24
	785 KN	Q25	Q26	Q27	Q28	Q29	Q30	Q31	Q32	Q33	Q34	Q35	Q36	Q37	Q38	Q39	Q40	Q41	Q42	Q43	Q44	Q45	Q46	Q47	Q48
	1157 KN	Q49	Q50	Q51	Q52	Q53	Q54	Q55	Q56	Q57	Q58	Q59	Q60	Q61	Q62	Q63	Q64	Q65	Q66	Q67	Q68	Q69	Q70	Q71	Q72
	SUBTITLE	Crack in the punch radius			Material sliding into the die (without crack)						Crack in the die shoulder						Crack in the drawbead			Crack between the drawbead and the die shoulder					

die shoulder, the region between the die shoulder and the drawbead, and the drawbead itself. The rejected specimens tested with the triangular drawbead, presented the crack on the die shoulder for 569 kN and in the drawbead for the 569 and 1157 kN conditions. Using the square drawbead, the rejected specimens presented the crack preferentially in the region between the drawbead and the die shoulder, except for the specimens with a width of 70 mm, for which the crack was located in the die shoulder to the 569 and 785 kN BHFs. From the resulted crack mapping, the effect of the sheet flow lines on the crack location is evident. In smaller width specimens, which simulate the deformation mode by deep drawing, the flow lines are less uniform than in larger width specimens, whose BHF actuation occurs in the entire perimeter around the stamped region. The less uniform the flow lines are, the stress concentration points are generated in the regions of discontinuity of flow, leading to cracking outside the deformation region of the stamped sample. This effect, added to the variation in the restriction imposed on the sheet by the different drawbead geometries and different BHF, led to the variation in the crack position shown in the mapping of Table 2.

3.2 FLC for different drawbead geometries

The circle dimensions at and near the fracture region were measured for the specimens for which the fracture occurred in the punch radius region (indicated by the green color in Table 2). The circle dimensions were then converted to the true strain and FLC were obtained for each drawbead geometry and for the three pre-defined BHF, totaling 12 FLC curves.

Thus, a first grouping of curves was carried out for comparative analysis of the formability. In this first analysis, a graph was generated for each drawbead geometry, where the curves for the BHF of 569, 785, and 1157 kN generated for the respective geometries were allocated in Fig. 8. Following this organization, Fig. 5a shows the FLCs for the flat drawbead, with 569, 785, and 1157 kN BHF conditions. Figure 5b shows the FLCs for the circular drawbead for the same BHF, while Fig. 8c, d show the FLCs for the triangular and square drawbead geometries for BHF of 569, 785 and 1157 kN, respectively. In this way, it is possible to analyze the influence that the BHF exerts on the formability of DP780 steel for each drawbead geometry used in the stamping tests.

According to Fig. 8, it is noted that all geometries presented lower formability for the 569 kN BHF and higher formability when using a load of 1157 kN, following the same results obtained by Chemin Filho et al. [31] for DP600 steel stamped without drawbead. These results attest to what Chemin Filho et al. [31] observed in his work where for very low BHF, below a certain critical value, the flow of the sheet metal becomes very accentuated, so that the portion of the sample hardened in the flange and shoulder region of the die advances too far into the stamping region of the sheet compromising the steel formability limit. The consequence of this is portrayed in a lower FLC curve, as occurred for the load of 569 KN, regardless of the drawbead geometry used in the tests.

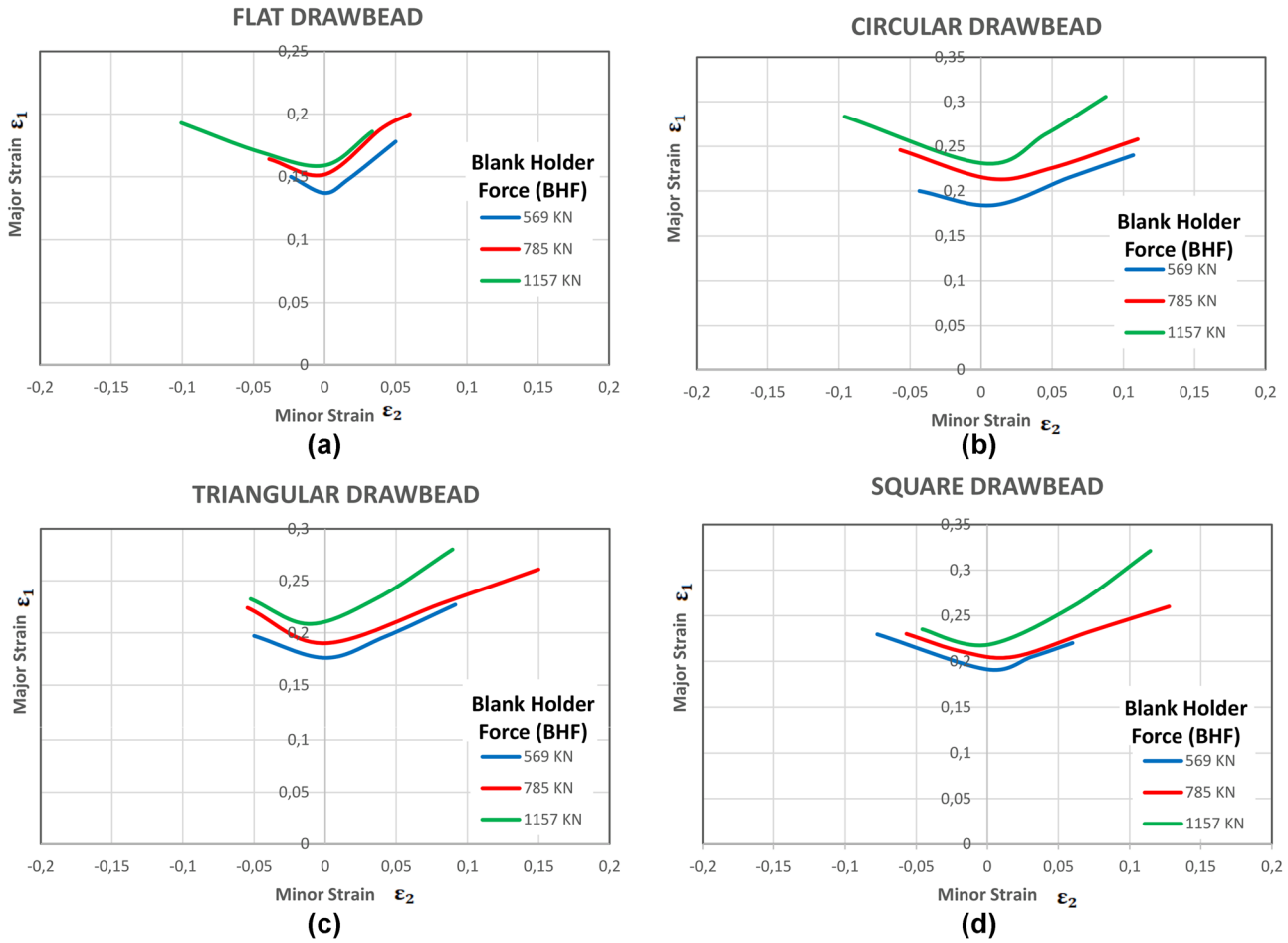

Fig. 8 Influence of the BHF on the formability of DP780 steel: **a** flat, **b** circular, **c** triangular, and **d** square drawbead geometry

The FLC curves, represented in Fig. 8a, show that the BHF has an influence on the stampability of DP780 steel. The tests proved that the smaller the BHF used, there is a tendency for the material to slip into the die reducing its stamp-ability limit. For this reason, an increase in the BHF, from 569 to 785 kN and later to 1157 kN, resulted in a considerable improvement in the material's stamp-ability, i.e., raising the major true strain, in the plane strain state, from 0.14 (569 kN) to 0.17 for 1157 kN. Figure 8b presents the results of the tests performed with the circular drawbead, repeating the BHF's of 569, 785, and 1157 kN. In this condition, the results were repeated; i.e., the higher the BHF, the greater the stampability limit of the material. In this case, however, compared to the test results with the flat drawbead, it was possible to verify a higher stampability limit in all BHF's, whose values in the plane strain state were between 0.18 and 0.23 for the 569 and 1157 kN conditions, respectively. Based on these results, it can be said that the effect of the circular drawbead in the material flow during stamping was beneficial for the DP780 steel, raising its maximum stampability limit by more than 40%.

Figure 8c shows the FLCs obtained with the triangular drawbead. For this geometry, the stamp-ability limit of the material was higher than the stamp-ability limit reached with the flat drawbead. The values of the major true strain in the plane strain state were between 0.18 and 0.21 for the forces of 569 and 1157 kN, respectively, slightly lower than the values obtained with the circular drawbead (approximately 8%). The FLCs obtained with the square drawbead, Fig. 8d, follow the same trend, i.e., the higher the BHF, the greater the stampability limit of the material. In the region of plane strain, the FLC presented the following values for the major true strain: 0.19, 0.2, and 0.22 for BHF of 569, 785, and 1157 kN, respectively. In this condition, the maximum stampability with square drawbead was approximately 4% lower than the limit reached with circular drawbead and approximately 4% higher than the formability with triangular drawbead. In resume, this first analysis is concluded, which indicates the best performance in formability of the

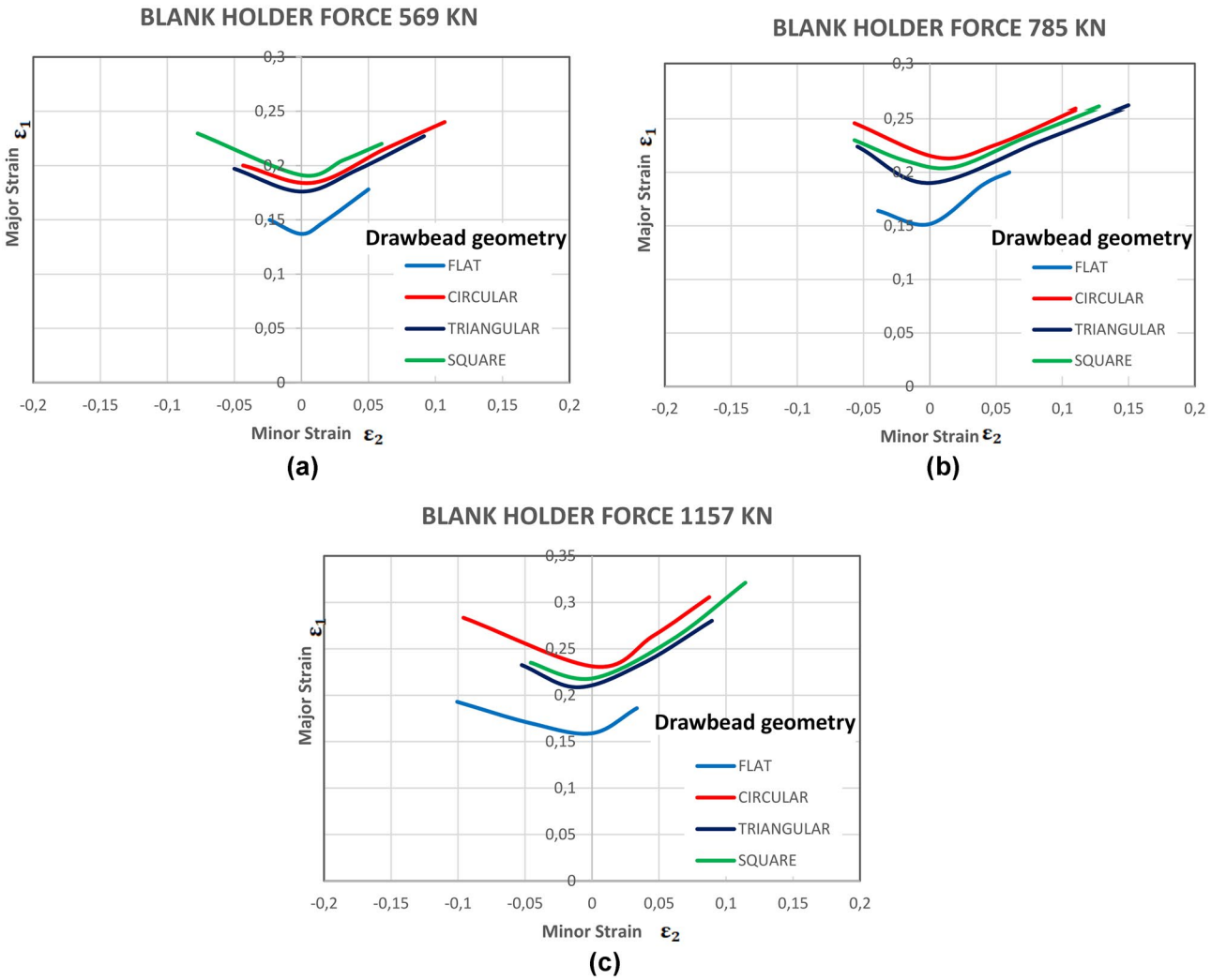

Fig. 9 Influence of drawbead geometry on stamping with BHF of **a** 569 kN, **b** 785 kN, and **c** 1157 kN

DP780 steel when stamped with the circular drawbead and BHF of 1157 kN. It should be noted, however, that all drawbead geometries (circular, triangular, and square) raised the stampability limit of DP 780 steel, demonstrating the real benefit of using this component for a better use of the sheet metal formability.

3.3 FLC for different BHFs

Another method of analyzing the results of the FLCs was the comparison of the curves generated for each BHF individually. In this case, the curves of each drawbead geometry used were grouped in the same graph, for the same BHF, Fig. 9.

In a general analysis of Fig. 9, it can be observed that the flat drawbead presented the worst formability for the three BHF (569, 785, and 1157 kN), with the FLC far below the curves obtained for the others drawbead geometries. It is also observed that the triangular drawbead presented a formability always lower than the circular and square geometries, however, not far from them. It is also noted that the circular drawbead presented the highest formability for the 785 and 1157 kN BHF, while, for the BHF of 569 kN, the highest formability limit was reached by the square drawbead.

In view of these data, the detrimental effect of the low restriction to the material flow in the flange region (for its formability) is again evident, since the flat geometry, which less restricts the flow of the sheet during stamping, originated lower FLCs. In this way, the restrictive function to the sheet flow, resulting from the use of the drawbead, substantially improves the formability limit of the steel by approximately 26, 31, and 30%, for the BHF of 569, 785, and 1157 kN, respectively.

In Fig. 9a, for the BHF of 569 kN, the drawbead geometry with the best stamp-ability was the square one, followed by circular and triangular ones, with very close values for

the major true strain: 0.19, 0.18, and 0.17, respectively (plane-strain state). The flat geometry, with a major true strain of approximately 0.14 (plane-strain state), was far below the others due to excessive flow of the sheet into the die, which, according to Chemin Filho [23], implies the advancement of hardened portions of the material on the die shoulder to the region of greatest deformation of the sample, compromising its stamp-ability. Still, in Fig. 9a, for BHF of 569 kN, it is noteworthy that the square drawbead presented greater formability than the circular drawbead. This result occurred because the low restriction to the flow of the sheet by the force of the blank holder was compensated by the greater restriction to the material flow imposed by the square drawbead when compared to the circular one. In other words, there was a compensation for the loss of formability due to low BHF by a drawbead geometry more restrictive to the flow.

For the tests with the BHF of 785 kN, Fig. 9b, the circular geometry stands out with the highest stamp-ability, reaching a major true strain of 0.22 in the plane strain state. In this same region, the stamping tests showed a major true strain of 0.20, 0.19, and 0.15 for drawbeads with square, triangular, and flat geometry, respectively. If we compare the maximum strain reached in the plane strain state, for the BHF of 569 and 785 kN, there was an increase in the formability limit of 13.6% with the BHF of 785 kN.

By the FLCs of Fig. 9c, it is observed again that the circular drawbead promoted the highest stampability, reaching a major true strain of 0.23 (plane strain state). This result characterizes a 4.35% increase in the formability limit with the increase in BHF from 785 to 1157 kN.

As the most striking aspect is that, through the analysis and discussion of the experiments, it was observed that the best performance of the material is reached, in terms of its stampability, through the balance between BHF and drawbead geometry. Both variables imply a restriction on the sheet flow in stamping, and the interpolation between them is what determines the performance of the steel in the process. In this way, the ideal flow of raw material in the process is sought to achieve the best material formability.

4 Conclusion

Noticing the importance of the stamping tool variables and how it affects the stampability of the material by restricting the flow, the current work evaluates the effect of the drawbead geometry and the BHF on the DP780 steel stampability. Several aspects were evidenced through the obtained results. First of them was focused on the cracking position of the sample, where only the wider specimens show the successful result. In these cases, the crack was located in the radius region of the punch. For the intermediate widths, not all specimens presented the crack in this position, while most of the narrower specimens failed outside the punch radius position, being rejected for the forming limit curve construction. This fact highlights the catastrophic effect of a nonuniform flow of the sheet metal during stamping, since for narrow samples the drawbead, which does not act on the sides of the sheet allows a totally free flow in this region. Consequently, there was a premature cracking of the material, varying in position according to the degree of restriction imposed by the drawbead model and applied BHF.

Regarding the stampability of DP780 steel, it is concluded that the most efficient results were obtained with the BHF of 1157 kN, since, regardless of the drawbead geometry, it was in this load condition that the steel reached the highest levels of deformation. It can be said that the stampability limit of DP780 steel increased as the BHF was increased from 569 up to 1157 kN.

For the BHF of 1157 kN, the highest level of the sheet deformation was achieved with the circular drawbead, characterizing this configuration as the most efficient for the stampability of DP780 steel. In short, it can be said that the circular drawbead, with a BHF of 1157 kN, promotes the best balance between the material advance in the flange and the deformation of the sheet inside the tool, which defines the steel performance in stamping.

Funding This research was funded by the Siderurgica ArcelorMittal S/A (DP780 supply) and CNPq (Brazil).

Availability of data and material Not applicable.

Code availability Not applicable.

Declarations

Ethics approval Not applicable.

Consent to participate Not applicable.

Consent for publication Not applicable.

Conflict of interest The authors declare no competing interests.

References

1. Spreafico C (2021) Can modified components make cars greener? A life cycle assessment. J Clean Prod 307:127190. Elsevier BV. https://doi.org/10.1016/j.jclepro.2021.127190
2. Sun X, Meng F, Liu J, Mckechnie J, Yang J (2019) Life cycle energy use and greenhouse gas emission of lightweight vehicle – a body-in-white design. J Clean Prod 220:1–8. Elsevier BV. https://doi.org/10.1016/j.jclepro.2019.01.225
3. Sun X, Liu J, Lu B, Zhang P, Zhao M (2017) Life cycle assessment-based selection of a sustainable lightweight automotive

engine hood design. Int J Life Cycle Assess 22(9):1373–1383. Springer Science and Business Media LLC. https://doi.org/10.1007/s11367-016-1254-y
4. Pattarakunnan K, Galos J, Das R, Mouritz AP (2021) Impact damage tolerance of energy storage composite structures containing lithium-ion polymer batteries. Compos Struct 267:113845. Elsevier BV. https://doi.org/10.1016/j.compstruct.2021.113845
5. Roy P, Tadele D, Defersha F, Misra M, Mohanty AK (2019) Environmental and economic prospects of biomaterials in the automotive industry. Clean Technol Environ Policy 21(8):1535–1548. Springer Science and Business Media LLC. https://doi.org/10.1007/s10098-019-01735-8
6. Vita A, Castorani V, Germani M, Marconi M (2019) Comparative life cycle assessment of low-pressure RTM, compression RTM and high-pressure RTM manufacturing processes to produce CFRP car hoods. Procedia Cirp 80:352–357. Elsevier BV. https://doi.org/10.1016/j.procir.2019.01.109
7. Abeyrathna B et al. (2015) A first step towards a simple in-line shape compensation routine for the roll forming of high strength steel. Int J Mater Form 9(3):423–434. Springer Science and Business Media LLC. https://doi.org/10.1007/s12289-015-1238-7
8. Andrade SL, Batista JF, Taiss JM, Rosa LK (2000) ULSAB-AVC – O aço no automóvel do futuro: A estratégia da USIMINAS. In: 55º Congresso da Associação Brasileira de Metalurgia e Materiais, 2000, Rio de Janeiro, Anais... Rio de Janeiro, Julho
9. Barlo A, Sigvant M, Endelt B (2019) On the failure prediction of dual-phase steel and aluminium alloys exposed to combined tension and bending. Iop Conf Ser Mater Sci Eng 651:012030–12040. IOP Publishing. https://doi.org/10.1088/1757-899x/651/1/012030
10. Ke J et al (2018) Formability of sheet metal flowing through drawbead – an experimental investigation. J Mater Process Technol 254:283–293. Elsevier BV. https://doi.org/10.1016/j.jmatprotec.2017.11.051
11. Keeler S, Menachem K (2014) Advanced high-strength steels application guidelines. Worldautosteel. Disponivel em: . Acesso em: 2015
12. Haase OC (2017) (Porto Alegre). 3 7th S e N A F O R. Influência da geometria do quebra-rugas na factibilidade do processo de estampagem com base no Método dos Elementos Finitos: Influence of drawbead geometry on stamping feasibility based on Finite Elements Method. Disponível em: <http://www.2017.senafor.com/conteudo/view?ID_CONTEUDO=442>. Acesso em: 04 ago. 2017
13. Schmid H, Hetz P, Merklein M (2019) Failure behavior of different sheet metals after passing a drawbead. Procedia Manuf 34:125–132. Elsevier BV. https://doi.org/10.1016/j.promfg.2019.06.129
14. Keeler SP (1965) Determination of forming limits in automotive stampings. Sheet Met Ind 42:683–691
15. Goodwin GW (1968) Application os strain analyses to sheet metal forming problems in the press shop. Metall Italiana 60:764–774
16. Woodthorpe J, Pearce R (1969) The effect of r and n upon the forming limit diagrams of sheet metal. Sheet Metal Ind 1061–1067
17. Min J, Stoughton TB, Carsley JE, Lin J (2016) Compensation for process-dependent effects in the determination of localized necking limits. Int J Mech Sci 117:115–134. Elsevier BV. https://doi.org/10.1016/j.ijmecsci.2016.08.008
18. Affronti E, Merklein M (2017) Metallographic analysis of Nakajima tests for the evaluation of the failure developments. Procedia Eng 183:83–88. Elsevier BV. https://doi.org/10.1016/j.proeng.2017.04.015
19. Iquilio RA et al (2019) Novel experimental method to determine the limit strain by means of thickNess variation. Int J Mech Sci 153–154:208–218. Elsevier BV. https://doi.org/10.1016/j.ijmecsci.2019.01.036
20. Shinmiya T et al (2019) Investigation of crack prediction method using limiting surface strain in high-strength steel sheets. Iop Conf Ser Mater Sci Eng 651:012065–012080. IOP Publishing. https://doi.org/10.1088/1757-899x/651/1/012065
21. Norz R, Volk W (2019) Investigation of non-proportional load paths by using a cruciform specimen in a conventional Nakajima test. Iop Conf Ser Mater Sci Eng 651:012020–12030. IOP Publishing. https://doi.org/10.1088/1757-899x/651/1/012020
22. Jocham D, Gaber C, Böttcher O, Volk W (2015) Prediction of formability for multi-linear strainpaths. Proc FTF 2015:59–64
23. Chemin Filho RA (2011) Estudo da fratura de aços de nova geração DP600 através da variação de pressão no prensa-chapas. Tese de Doutorado em Engenharia Mecânica pela Universidade Federal do Paraná
24. Sarraf IS et al (2018) Numerical analysis of damage evolution and formability of DP600 sheet with an extended Rousselier damage model. Int J Solids Struct 134:70–88. Elsevier BV. https://doi.org/10.1016/j.ijsolstr.2017.10.030
25. Leocata S et al (2019) Influence of binder pressure zones on the robustness of restraining forces in sheet metal forming. Procedia Manuf 29:209–216. Elsevier BV. https://doi.org/10.1016/j.promfg.2019.02.128
26. Tigrinho LMV, Chemin Filho RA, Marconde PVP (2013) Fracture analysis approach of DP600 steel when subjected to different stress/strain states during deformation. Int J Adv Manuf Technol 69:1017–1024. https://doi.org/10.1007/s00170-013-5104-9
27. Weinmann KJ, Rosenberger AH, Sanchez LR (1988) The Bauschinger Effect of Sheet Metal Under Cyclic Reverse Pure Bending. Michigan Technological University
28. Paul SK (2021) Controlling factors of forming limit curve: a review. Adv Ind Manuf Eng. https://doi.org/10.1016/j.aime.2021.100033
29. ISO 12004–2 (2008) Metalic materials - sheet and strip - determination of forming-limit curve. European Committe for Standardization
30. Chemin Filho RA, Marcondes PVP (2008) True strain distribution profile on sheet metal using different punch geometries. J Braz Soc Mech Sci Eng 30:1–6
31. Chemin Filho RA, Valente Tigrinho LM, Barreto Neto RC, Marcondes PVP (2013) An experimental approach for blankholder force determination for DP600 with different material flow strain rates in the flange during stamping. Proc Inst Mech Eng Part B J Eng Manuf 227(3):417–422. SAGE Publications. https://doi.org/10.1177/0954405412471281